3D Cu Pyramid Array Grown on Planar Cu Foil for Stable and Dendrite-free Lithium Deposition

Yaohua LIANG [1], Teddrick SCHAFFER [3], Abdus SOBHAN [1], Matthew BIESECKER [3], Zhongjiu YANG [4], Chenyu HAN [5], Jie HU [6], Alevtina SMIRNOVA [2], Zhengrong GU [1] *

[1] *Department of Agricultural and Biosystems Engineering, South Dakota State University, Brookings, SD 57007, USA*
[2] *Department of Chemistry, Biology, and Health Sciences, South Dakota School of Mines and Technology, Rapid City, SD 57701, USA*
[3] *Department of Mathematics & Statistics, South Dakota State University, Brookings, SD 57007, USA*
[4] *Department of Mechanical Engineering, University of Texas at Dallas, Richardson, TX 75080, USA*
[5] *Department of Industrial and Systems Engineering, Rutgers University, New Brunswick, NJ, USA*
[6] *Department of Mechanical Engineering, University of Massachusetts Lowell, Lowell, MA, USA*

http://doi.org/10.5755/j02.ms.34077

Received 15 May 2023; accepted 25 July 2023

Lithium metal is recognized as the anticipated anode for rechargeable batteries because of its inherent physicochemical properties. Unfortunately, the industrialization of Li metal anodes (LMAs) has been entangled in some intractable problems stemming from the uncontrollable growth of Li dendrites, which could result in the issue of short-circuit, thereby leading to cell failure. Here, a three-dimensional structured Cu pyramid array (CPA@CF) is constructed on planar Cu foil (CF) by the simple electrodeposition method. Owing to the features of large surface area and 3D porous structure, the proposed CPA@CF not only can promote Li-ion diffusion and charge transfer, but also effectively slow down the volume change of Li. Consequently, an even and steady Li plating/stripping process up to 360 h is realized using such a CPA@CF current collector. The Li@CPA@CF|$LiFePO_4$ full cell achieves an excellent Coulombic efficiency (CE) of 99.3 % for 160 cycles at 0.3 C with a superior capacity retention of 84.2 %.

Keywords: Li metal anode, dendrite-free, current collector, three-dimensional, Cu array.

1. INTRODUCTION

With the expanding demand for electronic products, electric transportation, and the application of clean energy, a cost-effective and performance-enhanced solution is desired [1 – 4]. Li metal as an anode has been spotlighted since the 1960s by virtue of its lowest electrode potential of -3.04 V (vs. SHE) associated with the high capacity of 3860 mAh g^{-1}, which exceeds is more than ten times that of common graphite anode [5, 6]. However, the implementation of commercial Li metal anode has been impeded by its proneness to the generation of Li dendrite, and severe volume changes during the unceasing cycling process, which generally triggers the SEI (solid electrolyte interphases) film crack and further promotes the side reaction [7, 8]. Meanwhile, the ruptured SEI film causes that the exposed fresh Li metal reacts with the electrolyte, which accelerates the consumption of active materials. These can give rise to low Coulombic efficiency, relatively large interfacial resistance, and even short–circuit issues [9, 10].

Several solutions have been explored to surmount these obstacles. One strategy is to establish a steady electrode/electrolyte interface by tailoring the appropriate electrolytes, such as adding lithium iodide (LiI) [11], nitrofullerene [12] as an electrolyte additive, thus activating a robust SEI film to protect Li metal. Employing artificial SEI film, such as LiF layer [13], and Li_2S/Li_2Se protection layer [14], is another strategy. These strategies undoubtedly can form stable interfaces and lessen relentless consumption of active Li. Nevertheless, the optimized SEI layer is not firm enough to stifle the volume expansion of active materials during the Li cycling process. Beyond that, utilizing a 3D conductive host, such as Ni_3S_2@3D host [15], Au nanoparticles@3D Ni foam [16], nanoporous $AuLi_3$ nanosheet-modified@Ni foam [17, 18], is a successful approach to postpone the volume change, constrain the growth of Li dendrite. As commercial anode current collectors, a tremendous amount of 3D porous Cu current collectors have been employed to store the active Li and block Li dendrite formation, such as lithiophilic layer modified 3D Cu foam [19], 3D Cu nanowires array [20]. However, the fabrication process of the aforementioned strategies is complicated and expensive, thus restricting their large-scale commercialization. Consequently, adopting a straightforward, facile, and inexpensive synthesis approach for the construction of current collectors is imperative.

Herein, we synthesized a pyramid-structured Cu array (CPA@CF) electrode for Li metal anodes employing the facile electrodeposition method. In comparison with planar Cu foil (CF), nano-pyramids of CPA@CF interleaved stacked to constitute 3D porous structures, which can enlarge the surface area, postpone the disordered expansion of Li and curb Li dendrite growth. Owing to these properties, CPA@CF based electrode exhibits extremely low overpotential, superior Coulombic efficiency (CE) and

* Corresponding author. Tel.: +1-605-688-5372.
E-mail: *zhengrong.gu@sdstate.edu* (Z. Gu)

durable cycling stability up to 360 h. In addition, Li@CPA@CF based full cell also demonstrates outstanding cycling stability and rate properties.

2. EXPERIMENTAL

Synthesis of Cu Pyramid Array/Cu foil: The copper foils were immersed in acetone, ethanol, 0.8 M H_2SO_4 and deionized water, sequentially, with ultrasonic treatment for 20 min, and then dried at 60 °C for 30 min. The Cu Pyramid Array (denoted as CPA@CF) was prepared in a three-electrode setup using the Pt-coated Ti mesh as the counter electrode, SCE as the reference electrode and as-pretreated samples (1*2.5 cm) as the working electrode with a 1 cm^2 area soaked in the plating solution, which consisting of $CuSO_4 \cdot 5H_2O$ (26 mM), $NiSO_4 \cdot 6H_2O$ (2 mM), $NaH_2PO_2 \cdot H_2O$ (200 mM), $Na_3C_6H_5O_7 \cdot 2H_2O$ (30 mM) and polyethylene glycol (8 mg L^{-1}). Potentiostatic electrodeposition was implemented at -1.00 V for 10 min by utilizing the electrochemical instrumentation (CHI760E, CH Instruments, Inc.). The as-prepared samples were washed with deionized water and dried at 60 °C for 30 min.

Material characterization: The scanning electron microscopy (Thermo Scientific™ Helios™ 5 CX Dual Beam field emission system with STEM-in-SEM and a full Oxford AZtec EDS, and FESEM, Hitachi, S–4700) was used to capture SEM, STEM images and EDX elemental mapping results of electrodes and characterize the morphological evolution of lithium deposited on the samples. The X-ray Powder diffractometer (Rigaku Ultima-Plus) was used to identify the elements of the samples.

Electrochemical measurements: The CR2032-type coin cells were fabricated in an argon glovebox for the electrochemical properties testing of the samples. Coulombic Efficiency measurements and long-term Li plating/stripping process evaluations under different testing conditions at 25 °C were conducted by employing a NEWARE battery testing system. $LiFePO_4$ with an areal mass load of 3 mg cm^{-2} was adopted as the cathode material for the evaluation of the full cells. A certain amount of lithium metal (4 mAh cm^{-2}) was predeposited on the samples before assembling the full cell [16, 18]. The EIS analysis with a frequency range of 100 kHz-10 mHz and an amplitude of 5 mV was performed using a model CHI760E instrument.

3. RESULTS AND DISCUSSION

A relatively smooth and flat surface of the CF with a small amount of contamination was observed in Fig. 1 a – c. The CPA@CF possesses a nano–pyramid structure with ridges on the surface contour as exhibited in Fig. 1 e – f. These Cu pyramid arrays were interleaved stacked to generate a 3D porous structure, which leads to a larger surface area compared to planar CFs. The 3D porous structure owned by CPA@CF could sterically hamper the disordered expansion of Lithium and constrain the growth of Li dendrites. Also, the construction of the pyramid array amplifies the surface area of the substrates and diminishes the local current density of the electrodes during the Li cycling process. In Fig. 1 g, the three typical peaks of CPA@CF and CF are consistent and appear at 43.36, 50.32, 74.04°, respectively [21, 22]. These three typical peaks are completely aligned with the (111), (200), and (220) lattice planes of Cu, respectively, according to the standard spectrum of Cu (PDF, No.04-0836), which proves that CPA@CF is perfectly composed of Cu element and has not been oxidized. Meanwhile, EDS elemental mapping of CPA@CF indicates the existence of the element Cu, as exhibited in Fig. 1 h – j.

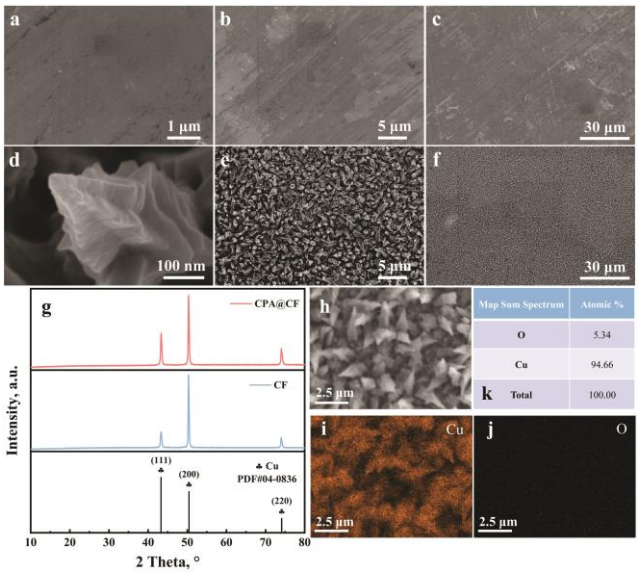

Fig. 1. a, b, c – SEM images of the bare CF; d, e, f – SEM images of CPA@CF; g – typical XRD pattern of CF and as prepared CPA@CF; h – SEM image of CPA@CF for EDS mapping; i – elemental mapping images of Cu; j – elemental mapping images of O; k – the atomic ratio of CPA@CF

SEM was exploited to observe the morphological evolution of Li metal plated on CF and CPA@CF (Fig. 2) at 1 mA cm^{-2} with different area capacity densities. At a charge amount stage of 0.4 mAh cm^{-2} (Fig. 2 a and e), a large number of pebbles-shaped lithium nuclei with erratic-size emerged on the surface of the planar CF. The shape of the Li metal gradually evolves to be more random as the deposition capacity increases (Fig. 2 b and c). Spaghetti–shaped lithium metal was observed at a charge capacity of 1.6 mAh cm^{-2}, as displayed in Fig. 2 d. The uncontrollable growth of Li dendrite on CFs can be attributable to the planar structure of the substrate and lithophobicity of Cu. In contrast, the morphology of Li metal plated on CPA@CF shows an obviously different evolution trend. The nano-pyramid structure is buried by the spherical lithium nuclei and the arrays structure on the substrate has dissipated at 0.4 mAh cm^{-2} [23]. The size and quantity of spherical lithium nuclei increase as the Li deposition is ongoing (Fig. 2 j and k). The morphology of lithium metal still maintains a regular ellipse shape, and no dendrites are generated when the charge capacity reaches 1.6 mAh cm^{-2}, as displayed in Fig. 2 l and p. The homogeneous Li distribution on CPA@CF benefits from the 3D porous structure of the Cu array, which is conducive to achieving an even electric field, and uniformly mediating the charge distribution. Fig. 2 q – r illustrates the behavior of Li plating on planar CF and CPA@CF. Li metal initially grows in an orientation away from the substrate surface and ultimately

produces Li dendrites and dead Li after cycling because of the disordered electric field caused by the innate lithiophobicity of copper.

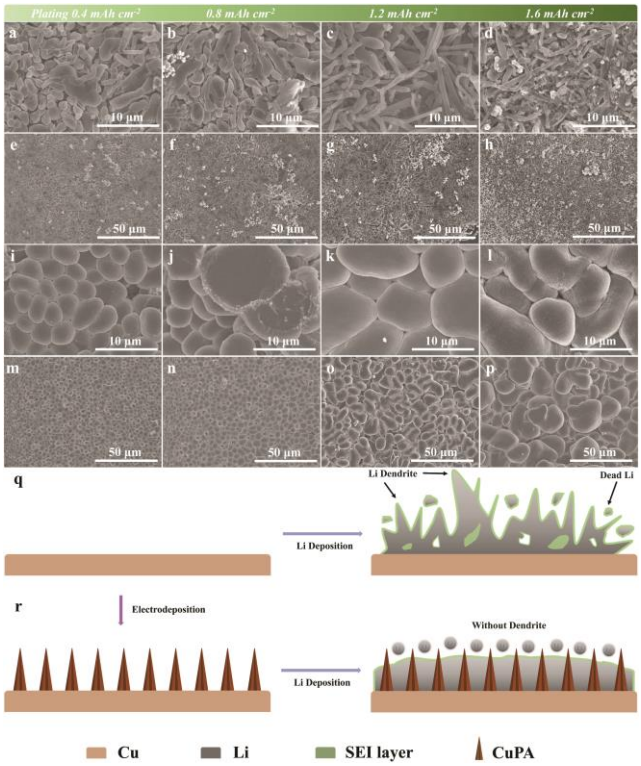

Fig. 2. a, b, c, d, e, f, g, h – SEM images of Li grown on the CF; i, j, k, l, m, n, o, p – SEM images of Li grown on the CPA@CF; q – illustration of Li growth behavior on CF; r – illustration of Li growth behavior on CPA@CF

The enormous Li dendrites generated after long-term cycling can stab the separator and trigger the occurrence of short circuits. By contrast, the CPA@CF current collector provides a 3D porous structure, which could facilitate the uniform growth of Li and the formation of the steady SEI film. Meanwhile, the infinite volume expansion of Li is significantly mitigated due to the structure of the Cu array, which also can considerably decrease the local current density and achieve Li homogenous deposition.

The nucleation overpotential can be denoted as the gap between the sharp drop of voltage at the initial stage of lithium nucleation and steady voltage plateau at the subsequent stage of further Li plating, which depends on the current density and the degree of lithiophilicity of the substrates [24]. The Li nucleation overpotential on the bare CF is 179.2 mV. In comparison, the Li nucleation overpotential on the CPA@CF is 49 mV, which manifests CPA@CF possesses a prominently low Li nucleation barrier, as shown in Fig. 3 a and b. To analyze the interfacial performance of two current collectors, EIS measurement was implemented. The diameter of the semicircle (R_{ct}) at the high–frequency regions reflects the interfacial resistance and the charge transfer resistance [25]. The planar CF exhibits a high R_{ct} value of 257 Ω before cycling, whereas the CPA@CF current collector displays a low R_{ct} value of 90.58 Ω before cycling (Fig. 3 c), and then it decreases to 29.53 Ω after 20 cycles, which is less than the R_{ct} value of 42.84 Ω of the CF after 20 cycles (Fig. 3 d). The lower R_{ct} value of the CPA@CF before cycling and after 20 cycles reveals a superior Li diffusion kinetics and a more stable SEI film during the cycling process.

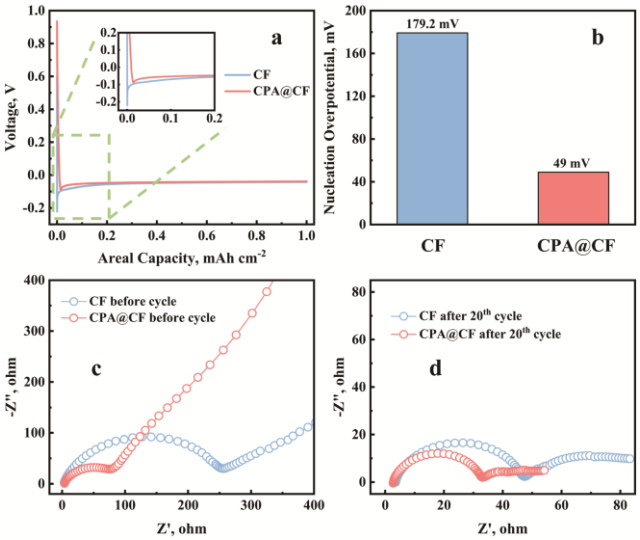

Fig. 3. a – nucleation overpotential of two type electrodes at 1 mA cm^{-2}; b – the corresponding histogram; c – EIS of CF and CPA@CF before cycle; d – EIS of CF and CPA@CF after 20 cycles at 1.5 mA cm^{-2}

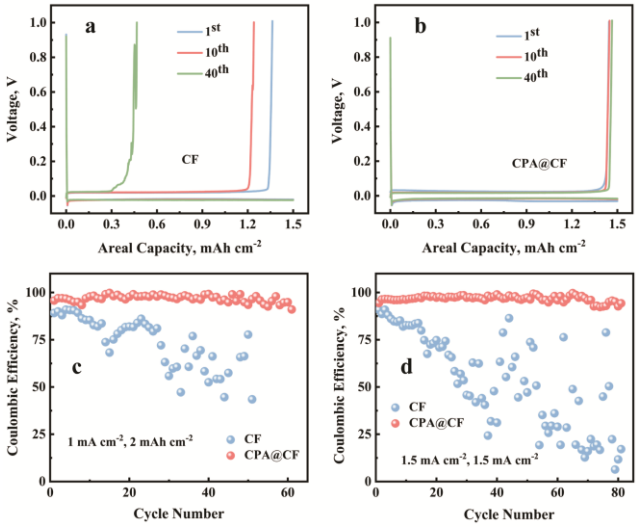

Fig. 4. a – voltage-areal capacity curves of CF; b – voltage-areal capacity curves of CPA@CF at 1.5 mA cm^{-2}; c, d – CEs of CF and CPA@CF at different testing conditions

The electrochemical properties of the CPA@CF current collector were assessed by Coulombic Efficiency (CE) testing. Fig. 4 a shows that the capacity of the reversible stripped Li decreases relatively after 10 cycles and reduces significantly after 40 cycles for the CF electrode, while the reversible charge capacity of CPA@CF has remained almost unchanged in subsequent cycling (Fig. 4 b). The planar CF shows a poor initial CE of 89.1 %, and the CE of the CF after 15 cycles slumps steeply to 68.2 % at 1 mA cm^{-2}. In contrast, the CPA@CF maintains an exceptional CE of 96.8 % over 61 cycles, as displayed in Fig. 4 c. The CE of CPA@CF remains at 94.3 % over 81 cycles, whereas the CE of bare CF displays dramatic degradation after 14 cycles at a different testing condition, as exhibited in Fig. 4 d. Obviously, the CE of CPA@CF is remarkably enhanced compared to planar CF. The inferior

CE performance of the CF can be blamed on the uncontrolled growth of Li dendrites, which gives rise to the rupture of the SEI, whereby the fresh Li metal reacts with the electrolyte, resulting in a large consumption of the active Li.

Moreover, the cycling stability of two current collectors was examined by assembling the CF and CPA@CF based symmetrical coin cells. CPA@CF based electrode exhibits a stable voltage curve without apparent voltage fluctuation at 1 mA cm^{-2}, as displayed in Fig. 5 a. At 1.5 mA cm^{-2}, the voltage-curve of the pristine CF shows a sharp ascent after 45 h, indicating an enlarging polarization inside the coin cell, and then an abrupt voltage fall appears after 119 h, resulting from the internal short–circuit and electrode failure, whereas the CPA@CF based electrode can cycle stably for 360 h without the issues of voltage oscillation and short-circuit, as exhibited in Fig. 5 b. This further proves that the CPA@CF current collector can stably operate at a relatively high current and capacity density and achieve stable charging and discharging cycling.

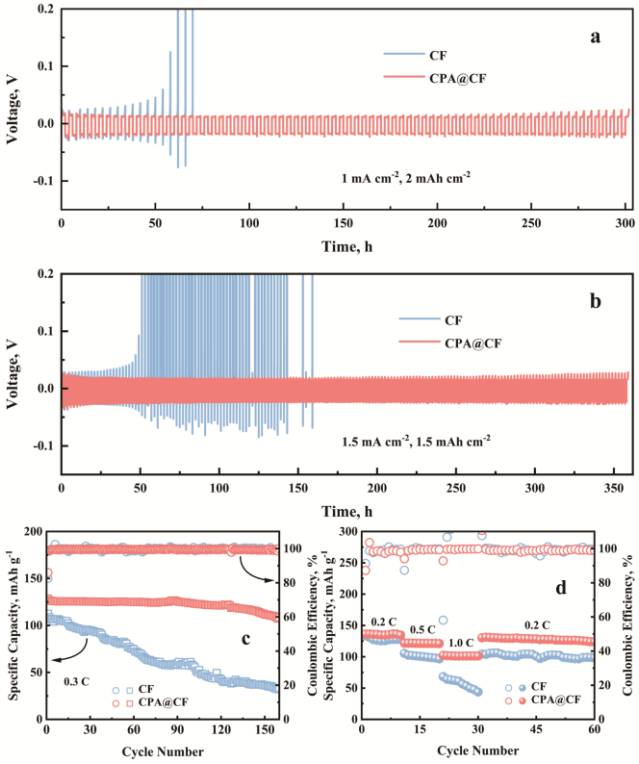

Fig. 5. a – voltage-time curves of CF; b – voltage-time curves of CPA@CF under different testing conditions; c – cycling performance of full cells; d – rate performance of full cells

To evaluate the commercial application of the proposed electrode, full cells were examined by pairing the Li pre-deposited CPA@CF with the $LiFePO_4$ cathode. Fig. 5c shows the CE of the Li@CF and Li@CPA@CF based full cells at 0.3 C for 160 cycles. The specific capacity of the Li@CF|$LiFePO_4$ decreases to 33.3 mAh g^{-1} after 160 cycles, while the specific capacity of the full cell with Li@CPA@CF retains at 108.2 mAh g^{-1} after 160 cycles, which is 84.2 % of its initial capacity. The rate performance of full cell with Li@CF or Li@CPA@CF was compared in Fig. 5 d. The capacity of CPA@CF based full cell is 135.6, 132.4 and 121.4 mAh g^{-1}, compared to 127.9, 100.7 and 50.7 of the CF based full cell, at 0.2, 0.5 and 1 C, respectively. Evidently, the CPA@CF based electrode demonstrates the excellent reversible specific capacity and outstanding capacity retention, proving the far–reaching impact of the CPA@CF electrode with the high surface area and porous structure on the electrochemical performance of the full cell.

4. CONCLUSIONS

In summary, we presented a Cu pyramid array/Cu foil (CPA@CF) composite synthesized by facile electrochemical deposition route and as a current collector to channel the Li uniform growth for dendrite–free Li metal battery. The CPA@CF possesses a 3D porous structure, which could greatly augment the surface area of the electrode and effectively lower current density. Meanwhile, the exclusive nano–pyramid structure of the CPA@CF provides an efficient porous path for Li–ion migration and interfacial charge transfer. Due to these positive characteristics, the CPA@CF electrode demonstrates a relatively low nucleation overpotential of Li deposition, superior CE of 94.3 % over 81 cycles and long cycling stability for over 360 h at 1.5 mA cm^{-2}. Moreover, the CPA@CF based full cell presents a superior cycling stability at 0.3 C and exceptional rate performance. Our study proffers a promising route to accomplish the practical application of LMAs in prospective energy storage devices.

Acknowledgments

This study was supported by the South Dakota "Governor's Research Center for Electrochemical Energy Storage", NSF EPSCoR South Dakota 2D Materials for Biofilm Engineering, Science and Technology Center (2DBEST) (No. OIA-1849206), USDA – Sungrant project "Advancing the Bioeconomy through Regional Sun Grant Centers (SA2000386): Production of 3D Graphene from Renewable Lignin Through Flash Catalytic Thermochemical Processes", USDA REEU "Sustainability of Agricultural Systems-Role of Interface and New Technology" (SA2000489), USDA Hatch (SD00H735–22) New Biorefinery: Value added Products from Biomass and Biotechnology of Sustainable Agriculture, USDA Multistate Hatch (SD00R679-19) "The Science and Engineering for a Biobased Industry and Economy", USDA Multistate Hatch (SD00R708-22) "Nanotechnology and Biosensors".

REFERENCES

1. **Wei, Z., Salehi, A., Lin, G., Hu, J., Jin, X., Agar, E., Liu, F.** Probing Li–Ion Concentration in an Operating Lithium Ion Battery Using in Situ Raman Spectroscopy *Journal of Power Sources* 449 2020: pp. 227361. https://doi.org/10.1016/j.jpowsour.2019.227361
2. **Liu G., Sun Z., Shi X., Wang X., Shao L., Liang Y., Lu X., Liu J., Guo Z.** 2D-Layer-Structure Bi to Quasi-1D-Structure $NiBi_3$: Structural Dimensionality Reduction to Superior Sodium and Potassium Ion Storage *Advanced Materials* 2023: pp. 2305551. https://doi.org/10.1002/adma.202305551
3. **Liang Y., Ding W., Yao B., Zheng F., Smirnova A., Gu Z.** Mediating Lithium Plating/Stripping by Constructing 3D Au@Cu Pentagonal Pyramid Array *Batteries* 9 2023: pp. 279.

https://doi.org/10.3390/batteries9050279
4. **Liang, Y., Ke, X., Liu, J., Shi, Z.** Preparation and Supercapacitive Performance of MnO_2@Nanoporous Gold/Ni Foam Electrode Materials *Energy Storage Science and Technology* 6 (S1) 2017: pp. 1 – 7. https://esst.cip.com.cn/CN/10.12028/j.issn.2095-4239.2017.0138
5. **Ke, X., Zhang, Z., Cheng, Y., Liang, Y., Tan, Z., Liu, J., Liu, L., Shi, Z., Guo, Z.** $Ni(OH)_2$ Nanoflakes Supported on 3D Hierarchically Nanoporous Gold/Ni Foam as Superior Electrodes for Supercapacitors *Science China Materials* 61 (3) 2017: pp. 353 – 362. https://doi.org/10.1007/s40843-017-9144-8
6. **Zhang, Y., Wei, C., Sun, J., Jian, J., Jin, C., Lu, C., Peng, L., Li, S., Rümmeli, MH., Yang, R.** Au@rGO Modified Ni Foam as a Stable Host for Lithium Metal Anode *Solid State Ionics* 364 2021: pp. 115636. https://doi.org/10.1016/j.ssi.2021.115636
7. **Cho, K.Y., Hong, S.H., Kwon, J., Song, H., Kim, S., Jo, S., Eom, K.** Effects of a Nanometrically Formed Lithiophilic Silver@Copper Current Collector on the Electrochemical Nucleation and Growth Behaviors of Lithium Metal Anodes *Applied Surface Science* 554 2021: pp. 149578. https://doi.org/10.1016/j.apsusc.2021.149578
8. **Liu, G., Wang, N., Qi, F., Lu, X., Liang, Y., Sun, Z.** Novel Ni–Ge–P Anodes for Lithium–Ion Batteries with Enhanced Reversibility and Reduced Redox Potential *Inorganic Chemistry Frontiers* 10 (2) 2023: pp. 699 – 711. https://doi.org/10.1039/d2qi01973f
9. **Cai, Y., Qin, B., Li, C., Si, X., Cao, J., Zheng, X., Qi, J.** Stable Lithium Metal Anode Achieved by Shortening Diffusion Path on Solid Electrolyte Interface Derived from Cu_2O Lithiophilic Layer *Chemical Engineering Journal* 433 2022: pp. 133689. https://doi.org/10.1016/j.cej.2021.133689
10. **Liu, G., Yang, Y., Lu, X., Qi, F., Liang, Y., Trukhanov, A., Wu, Y., Sun, Z., Lu, X.** Fully Active Bimetallic Phosphide $Zn_{0.5}Ge_{0.5}P$: A Novel High–Performance Anode for Na–Ion Batteries Coupled with Diglyme–Based Electrolyte *ACS Applied Material Interfaces* 14 (28) 2022: pp. 31803 – 31813. https://doi.org/10.1021/acsami.2c03813
11. **Wang, G., Xiong, X., Xie, D., Fu, X., Ma, X., Li, Y., Liu, Y., Lin, Z., Yang, C., Liu, M.** Suppressing Dendrite Growth by a Functional Electrolyte Additive for Robust Li Metal Anodes *Energy Storage Materials* 23 2019: pp. 701 – 706. https://doi.org/10.1016/j.ensm.2019.02.026
12. **Jiang, Z., Zeng, Z., Yang, C., Han, Z., Hu, W., Lu, J., Xie, J.** Nitrofullerene, a C_{60}–based Bifunctional Additive with Smoothing and Protecting Effects for Stable Lithium Metal Anode *Nano Letters* 19 (12) 2019: pp. 8780 – 8786. https://doi.org/10.1021/acs.nanolett.9b03562
13. **Lang, J., Long, Y., Qu, J., Luo, X., Wei, H., Huang, K., Zhang, H., Qi, L., Zhang, Q., Li, Z., Wu, H.** One–Pot Solution Coating of High Quality LiF Layer to Stabilize Li Metal Anode *Energy Storage Materials* 16 2019: pp. 85 – 90. https://doi.org/10.1016/j.ensm.2018.04.024
14. **Liu, F., Wang, L., Zhang, Z., Shi, P., Feng, Y., Yao, Y., Ye, S., Wang, H., Wu, X., Yu, Y.** A Mixed Lithium–Ion Conductive Li_2S/Li_2Se Protection Layer for Stable Lithium Metal Anode *Advanced Functional Materials* 30 (23) 2020: pp. 202001607. https://doi.org/10.1002/adfm.202001607
15. **Fan, Y., He, X., Li, H., Huang, Y., Sun, C., Liu, H., Huangzhang, E., Sun, F., Zhao, X., Nan, J.** Lithiophilic Ni_3S_2 Layer Decorated Nickel Foam (Ni_3S_2@Ni Foam) with Fast Ion Transfer Kinetics for Long–Life Lithium Metal Anodes *Chemical Engineering Journal* 450 2022: pp. 138384. https://doi.org/10.1016/j.cej.2022.138384
16. **Ke, X., Liang, Y., Ou, L., Liu, H., Chen, Y., Wu, W., Cheng, Y., Guo, Z., Lai, Y., Liu, P., Shi, Z.** Surface Engineering of Commercial Ni Foams for Stable Li Metal Anodes *Energy Storage Materials* 23 2019: pp. 547 – 555. https://doi.org/10.1016/j.ensm.2019.04.003
17. **Chen, Y., Ke, X., Cheng, Y., Fan, M., Wu, W., Huang, X., Liang, Y., Zhong, Y., Ao, Z., Lai, Y., Wang, G., Shi, Z.** Boosting the Electrochemical Performance of 3D Composite Lithium Metal Anodes Through Synergistic Structure and Interface Engineering *Energy Storage Materials* 26 2020: pp. 56 – 64. https://doi.org/10.1016/j.ensm.2019.12.023
18. **Liang, Y., Chen, Y., Ke, X., Zhang, Z., Wu, W., Lin, G., Zhou, Z., Shi, Z.** Coupling of Triporosity and Strong Au–Li Interaction to Enable Dendrite–Free Lithium Plating/Stripping for Long–Life Lithium Metal Anodes *Journal of Materials Chemistry A* 8 (35) 2020: pp. 18094 – 18105. https://doi.org/10.1039/d0ta04768f
19. **Wang, J-r., Wang, M-m., He, X-d., Wang, S., Dong, J-m., Chen, F., Yasmin, A., Chen, C-h.** A Lithiophilic 3D Conductive Skeleton for High Performance Li Metal Battery *ACS Applied Energy Materials* 3 (8) 2020: pp. 7265 – 7271. https://doi.org/10.1021/acsaem.0c00055
20. **Tan, L., Li, X., Cheng, M., Liu, T., Wang, Z., Guo, H., Yan, G., Li, L., Liu, Y., Wang, J.** In–situ Tailored 3D Li_2O@Cu Nanowires Array Enabling Stable Lithium Metal Anode with Ultra–High Coulombic Efficiency *Journal of Power Sources* 463 2020: pp. 228178. https://doi.org/10.1016/j.jpowsour.2020.228178
21. **Cao, J., Deng, L., Wang, X., Li, W., Xie, Y., Zhang, J., Cheng, S.** Stable Lithium Metal Anode Achieved by In Situ Grown CuO Nanowire Arrays on Cu Foam *Energy & Fuels* 34 (6) 2020: pp. 7684 – 7691. https://doi.org/10.1021/acs.energyfuels.0c01180
22. **Qiu, H., Tang, T., Asif, M., Huang, X., Hou, Y.** 3D Porous Cu Current Collectors Derived by Hydrogen Bubble Dynamic Template for Enhanced Li Metal Anode Performance *Advanced Functional Materials* 29 (19) 2019: pp. 1808468. https://doi.org/10.1002/adfm.201808468
23. **Diao, W.Y., Xie, D., Li, Y.F., Jiang, R., Tao, F.Y., Sun, H.Z., Wu, X.L., Zhang, X.Y., Zhang, J.P.** Sustainable and Robust Graphene Cellulose Paper Decorated with Lithiophilic Au Nanoparticles to Enable Dendrite–free and High-Power Lithium Metal Anode *Chemistry–A European Journal* 27 (31) 2021: pp. 8168 – 8177. https://doi.org/10.1002/chem.202100440
24. **Xie, Y., Zhang, H., Yu, J., Liu, Z., Zhang, S., Shao, H., Cao, Y., Huang, X., Li, S.** A Novel Dendrite–Free Lithium Metal Anode via Oxygen and Boron Codoped Honeycomb Carbon Skeleton *Small* 18 (11) 2022: pp. e2104876. https://doi.org/10.1002/smll.202104876
25. **Wu, Q., Qin, M., Yan, H., Zhong, W., Zhang, W., Liu, M., Cheng, S., Xie, J.** Facile Replacement Reaction Enables Nano-Ag-Decorated Three-Dimensional Cu Foam as High–Rate Lithium Metal Anode *ACS Applied Materials Interfaces* 14 (37) 2022: pp. 42030 – 42037. https://doi.org/10.1021/acsami.2c10920